Mode-locking transitions and vortex flows in current-driven Josephson-junction arrays

Shantilal Das and Deshdeep Sahdev
Department of Physics, Indian Institute of Technology, Kanpur-208 016, India

Ravi Mehrotra
National Physical Laboratory, Dr. K. S. Krishnan Road, New Delhi 110 012, India

(Received 12 August 1996; revised manuscript received 15 October 1996)

The dynamical behavior of overdamped dc-driven Josephson-junction arrays is studied numerically in two dimensions. Currents varying linearly along an edge are injected into the array and drawn out at the opposite edge either uniformly or through a busbar. The system is found to undergo a series of dynamical transitions as the gradient of the current drive is increased. We show that, for ladder arrays, these transitions mark the loss of mode locking across specific bonds. The transitions can, alternatively, be associated with the onset of well-defined vortex flows. Spatial localization of vortices in individual plaquettes of a ladder, driven in the direction of its length, is seen to stablize quasiperiodicity of order $N>3$ in a certain region of the underlying parameter space. We also discuss the extension of each of these features to full-fledged rectangular arrays. [S0163-1829(97)04110-6]

I. INTRODUCTION

It has long been believed that the dynamics of complex systems is, in large part, determined by that of their collective excitations. For example, in hydrodynamics, vortices and structures using vortices as building blocks, enter crucially into descriptions of the system's behavior in different dynamical regimes.[1] Two-dimensional (2D) Josephson-junction arrays (JJA's) provide somewhat simpler experimental systems in which this belief can be critically examined *and* articulated. They are simpler because the basic variables are, first, angular (i.e., confined to $(-\pi,\pi]$) and, second, defined only on a 2D lattice. Several authors have, accordingly, studied current-driven JJA's numerically, keeping track of vortices, which are the relevant collective excitations.[2–7] Mehrotra and Shenoy[2,3] have pictured the onset of turbulence in nonuniformly driven JJA's at zero temperature in terms of the mixing of vortices at the current-driven edge. Xia and Leath[4,5] have studied current flow past linear defects and found that a periodic flow of vortices in the central defect corridor (CDC) marks the transition from fixed-point to limit cycle behavior. Moreover, the nucleation and flow of vortices, for large input currents, in columns adjoining the CDC produce quasiperiodic and chaotic behaviors. This investigation was carried forward by Datta *et al.*,[8] who accessed and explored the multiple-vortex fixed-point sectors of these arrays by extending the size of both array and defect.

A second approach to the dynamics of JJA's results if we view them as sets of globally coupled nonlinear oscillators,[9–17] which tend to rotate in a mode-locked fashion unless driven by highly unequal torques. The motion of these systems is restricted to N tori and has been extensively studied.[18–20] As a result, the $N=2$ case has come to be well understood (it gives rise to only two types of flows—periodic and quasiperiodic), and a number of facts have been discovered about the $N\geqslant 3$ case.[16,21–25] In particular, it has been shown[23,24] that for a system with a three-frequency quasiperiodic (QP^3) attractor, there exist arbitrarily small C^2 perturbations,[26] which convert the attractor to one which is strange and structurally stable. For $N\geqslant 4$, these perturbations can be chosen to be C^∞. The existence of these perturbations notwithstanding, the occurrence of chaos in these systems is actually quite rare. Indeed, applying nonlinear perturbations to maps on N tori, Grebogi, Ott, and Yorke[25] found that, for small to moderate nonlinearity, the attractors encountered, ordered through frequency of occurrence, are QP^N, QP^{N-1}, . . . , QP^1 equivalent to P (periodic). The chaotic attractor is seen very seldom for $N=3$ but slightly more often for $N=4$. For larger nonlinearity, QP^N becomes less common and disappears altogether when the map becomes noninvertible. Finally, among different types of chaotic attractors, the most common are those whose limit set coincides with the N torus itself.

A detailed connection between the two approaches was established, for the simplest case of an overdamped triangular network.[18] The underlying parameter space was mapped and each region interpreted in terms of vortices. This analysis was subsequently extended to an *under*damped triangular network,[27] as well.

In this paper, we synthesize the insights produced by all these investigations into a single coherent picture. We work with uniform, defect-free, overdamped arrays subject to nonuniform dc drives, i.e., a current varying along the y direction is injected in the x direction at the $x=0$ edge of the array (see Fig. 1). A current drive has nonzero $\partial i_x/\partial y$ and hence carries a net vorticity. Since uniform drives applied to arrays with linear defects automatically become nonuniform, and maximally so at the CDC—the analog of the drive edge, the configuration we consider accords us a host of *general* dynamical insights at *minimal* computational cost. A further saving of computer time can be achieved by realizing that certain features of larger arrays are faithfully captured by smaller ones. Some of the features studied in this paper are, in fact, of precisely this type and we point this out wherever relevant. As for the choice of the nonuniform drive, we find

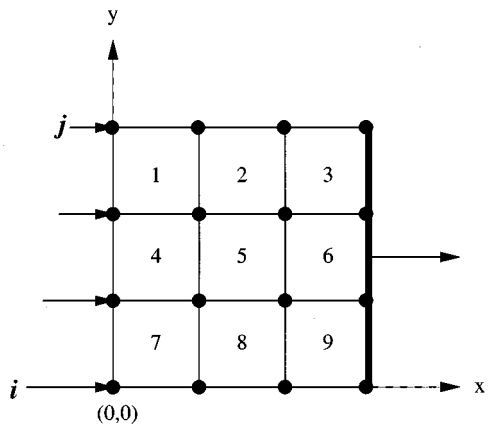

FIG. 1. Geometrical representation of a JJA with $N_x=N_y=4$. The dots denote the superconducting islands and the bonds denote Josephson junctions. A linearly varying dc current profile is applied at the $x=0$ edge. The $x=L_x$ edge is shorted by a busbar. The plaquettes are numbered as shown.

that, for the points we wish to make, a drive with a simple linear profile is sufficient. Finally, we emphasize that, since chaotic oscillations are altogether absent for individual dc-driven overdamped junctions, the observed *continuous* frequencies result exclusively from the interactions between junctions, which are the primary foci of this investigation.

The picture we develop can now be outlined. For low values of the input drive, the system displays fixed-point vortex-free behavior. Time dependence first results from the flow of vortices, which enter through one of the nondriven free boundaries, travel along a column and leave the array at the opposite edge. (This process can equivalently be described as the nucleation and annihilation of vortices and *image* antivortices at the array boundaries). Each frequency seen in the Fourier transform of any voltage time series is associated with one such vortex flow. As long as the injected vorticity is small, the junctions along each column of the array remain 1/1 mode locked. Locking of this type turns the associated bonds separating the columns, effectively into closed gates for vortices. All vortex flows thus occur columnwise at this point, the corresponding frequencies remain spatially separated and, for an array of N columns, the attractor is QP^N. With increasing vorticity of the input, some of the junctions along the drive edge come mode unlocked, and vortices begin to flow through the corresponding bonds in the direction of the external current. This leads to flows which mix and generate an infinite range of incommensurate frequencies, and hence chaos. To the extent that junctions away from the drive edge are still mode locked at this stage, the flow and mixing of vortices can be spatially isolated. As further mode-locking transitions occur, the region of mixing extends deeper into the array.

With the help of this picture, we have been able to plot the phase diagram of our system, with a reasonable degree of resolution. For some small arrays we have, in fact, seen Arnold tongues merging and overlapping to produce chaos. We should mention that although parts of this picture were anticipated in Ref. 3, the mode locking between junctions, as also its connection with vortex flows and with features of the associated phase diagram were missed altogether.

The paper is organized as follows. We discuss the model system and the governing equations in Sec. II. Investigations for ladder arrays are carried out in Sec. III. The cases of vertical (Sec. III A) and horizontal ladders (Sec. III B) relative to the current applied in the x direction are studied separately. In Sec. III C, the possibility of higher-order quasiperiodicity in ladder arrays is discussed. We extend some of the results for ladder arrays to general rectangular arrays in Sec. III D. Section IV contains a summary and discussion of our results.

II. THE MODEL

The equation governing the dynamics of a single overdamped resistively-shunted-Josephson junction (RSJ), linking superconducting sites r and s, at zero temperature and in zero magnetic field, is given by the RSJ model[28,29] as

$$\frac{d\phi_{rs}}{dt}+\sin\phi_{rs}=I_{rs}, \tag{1}$$

where $\phi_{rs}=\phi_r-\phi_s$ is the phase difference across the junction, and I_{rs} the total current carried by the bond rs. All currents are scaled in terms of the single junction critical current i_c, and time is expressed in units of $(\hbar/2eRi_c)$, R being the shunt resistance.

For an arbitrary array, this equation applies individually to each bond. Thus, for an $N_x\times N_y$ array of superconducting sites, connected by overdamped Josephson junctions, driven by external currents I^{ext}, the corresponding equations can be written using total current conservation[30] as

$$\sum_{\langle rs\rangle}\frac{d\phi_{rs}}{dt}+\sin(\phi_{rs})=I_r^{\mathrm{ext}} \quad \forall r \tag{2}$$

where $\langle rs\rangle$ implies that the sum is over nearest neighbors of r. Note that ϕ_{rs} and hence Eq. (1) are invariant under $\phi_r\rightarrow\phi_r+\alpha$, where α is a constant. In solving Eq. (2) numerically, it is important to eliminate this freedom. This can be done easily, for example, by setting the phase at an arbitrarily chosen site to zero.

Equation (2) can alternatively be written in terms of the discrete Laplacian G_0^{-1}, as

$$\sum_r (G_0^{-1})_{rs}\dot{\phi}_s=-d_r \tag{3}$$

where the divergence term at each site is given by $d_r=I_r^{\mathrm{ext}}-\Sigma_{\langle rs\rangle}\sin\phi_{rs}$.

For an array of size $N_x\times N_y\equiv N$, each integration time step of Eq. (3) has a complexity $\mathcal{O}(N^2)$ (since at every upgradation of the N phase variables, ϕ, the constant $N\times N$ matrix G_0 has to be multiplied by the divergence vector $[d]$). However, using the special properties of G_0^{-1}, faster algorithms have been evolved wherein the above multiplication is carried out in $\mathcal{O}(N\ln N)$ steps or faster.[31,32] Fast algorithms have also been developed for the case of busbars and defects in the form of missing bonds.[33] For small arrays with only a few plaquettes, we use the direct $\mathcal{O}(N^2)$ algorithm. Faster algorithms are resorted to only when studying larger arrays.

In this paper, we choose a transversely varying dc current drive $I_x(y)=i-\Delta y/L_y$, $\Delta=i-j$, applied to the $x=0$ edge of the array. The current thus varies linearly, from i at $y=0$ to j at $y=L_y$ (see Fig. 1). This is a simple form of nonuniformity. More complex nonuniform time-dependent current profiles exist in the neighborhood of defects (missing bonds) contained in uniformly driven arrays.

The choice of the drive made, the Laplacian matrix is inverted numerically, once and for all, for a given array size with a reference phase fixed to prevent the matrix G_0^{-1}, from becoming singular. We keep the phases all along the $x=L_x$ edge fixed at zero. Physically, this corresponds to shorting out these sites with a busbar. All other phases, including those at the free boundaries, $y=0$ and $y=L_y$, evolve according to the Eq. (3). The differential equations are integrated by a fourth order Adams-Moulton predictor-corrector routine. The integration time step chosen is 0.05 and the dynamics is studied for typically 10^5 integration steps per run (after discarding, typically, the first 10^4 steps, which correspond to transients).

We note that, $\Sigma\phi_{rs}=0$ identically, for a summation carried out around any closed path, or, in particular around a plaquette. If we restrict all phase differences to lie in the range $(-\pi,\pi]$ say, this condition must however be generalized to read $\Sigma\phi_{rs}=2\pi n$ $(n=-1,0,1)$. This is used to identify the existence of a vortex in a plaquette. The transversely varying current drive under consideration, injects vorticity $\partial I_x(y)/\partial y=-\Delta$ into the array. This manifests itself as a non-neutral system of vortices. For $\Delta>0$, these are predominantly positive.

III. THE DYNAMICS OF LADDER ARRAYS

As mentioned in the Introduction, the simplest network, namely one with $N_x=2$ and $N_y=2$ has been intensively studied in terms of both the basic phase variables and of vortices.[18] The i-Δ phase diagram consists of a fixed-point steady-state regime, and an infinity of Arnold tongues which merge at the steady-state boundary. The behavior in the regions separating the tongues is quasiperiodic with two independent frequencies. The quasiperiodicity is intermittent at the edges of the tongues.

In this section, we present results showing that many interesting features of the above configuration carry over to arrays of larger size. We do so by extending the single plaquette in the x and y directions separately before discussing full-fledged rectangular arrays.

A. $2\times N_y$ ladders

We begin with the simple $N_y=3$ case (see Fig. 2). We arbitarily choose the reference phase $\phi_0=0$ whence $\phi_{r0}=\phi_r\forall r$.

Since Eqs. (3) describing the evolution of the three phases ϕ_1, ϕ_2, and ϕ_3 are periodic in each phase with period 2π, the dynamics is confined to a three-dimensional toroidal phase space. Accordingly, three types of motion are possible for this system: coherent (periodic, or quasiperiodic with only two independent frequencies), QP^3 and chaotic. The first is characterized by two or more of the average rates of winding of the three phases, bearing a rational ratio to each other (voltage/frequency locking), i.e., $\langle\dot\phi_r\rangle/\langle\dot\phi_s\rangle=p/q$ (where $r,s=1,2,3$ and p, q are small integers). The second is characterized by all three winding rates bearing irrational ratios to one another, with motion regular in behavior and power spectra for time-dependent voltages discrete in frequency. The third, once again, has average rates of winding in irrational ratios to one another, but this is now accompanied by an apparent randomness of motion, noisy (continous) spectra, and a sensitivity to initial conditions (i.e., at least one positive Lyapunov exponent). In geometric terms, coherence corresponds to trajectories which form closed curves on the three torus or, when only two junctions are locked, closed curves in the 2D subspace of the pair of locked junctions. Triply periodic trajectories fill the entire three torus and are associated with volume conservation in time. Finally, chaotic motion results in strange attractors, i.e., an attractive set with fractal dimension and self-similar structure.

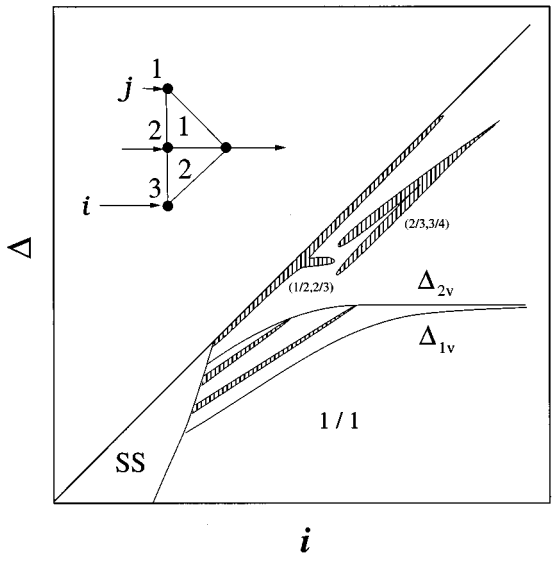

FIG. 2. Schematic phase diagram (not to scale) for a 2×3 configuration as depicted in the inset with the islands and plaquettes numbered as shown. The region marked SS is the steady-state region, while the region marked 1/1 represents voltage locking. The other frequency locked zones are shaded regions in the figure (only few of these are shown). For $\Delta_{1v}(i)<\Delta<\Delta_{2v}(i)$, they are characterized by two winding numbers (1/1, p_2/q_2) whereas for $\Delta>\Delta_{2v}$, they are of the type (p_1/q_1, p_2/q_2).

The behavior of the 2×3 system is represented schematically by the $i-\Delta(=i-j)$ phase diagram shown in Fig. 2. The region marked SS corresponds to the time-independent fixed-point regime where $\dot\phi_r=0\forall r$. The rest of the phase diagram is divided into various regions of frequency locking, quasiperiodicity, and chaos. The mode-locked behavior of the system in these regions warrants a detailed description.

In Fig. 3 we show the variation of the winding number $w_{rs}=\langle\dot\phi_r\rangle/\langle\dot\phi_s\rangle$ with the gradient of the applied current profile, Δ, for $i=1.8$. For $\Delta=0$, Eqs. (3) can readily be used to show that $\phi_1=\phi_2=\phi_3$ is a possible stable solution. We see that the phase-locked state ($w_{rs}=1$) from Fig. 3 persists stably over a fairly large interval in Δ. At a critical value, $\Delta=\Delta_{1v}(i)$, of the gradient, the locking between junctions 2-0 and 3-0 breaks and ω_{23} falls below unity. The junctions

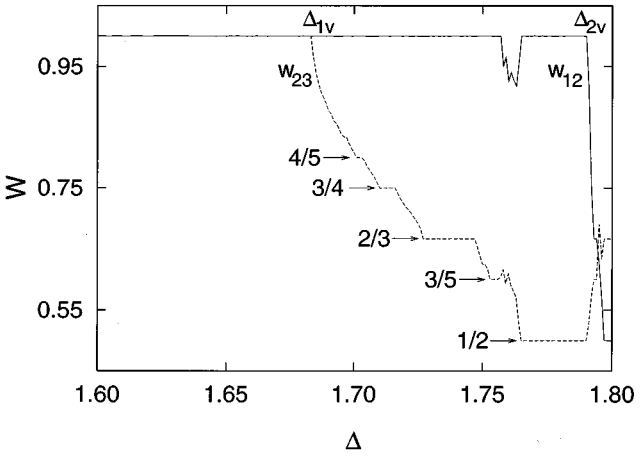

FIG. 3. Variation of the winding number $w_{rs}=\langle\dot{\phi}_r\rangle/\langle\dot{\phi}_s\rangle$ with the gradient Δ in a 2×3 array for $i=1.8$. The steps mark the periodic tongues with specific winding ratios shown against each step. Note that the axes do not start at zero. The locking of w_{23} and w_{12} breaks at Δ_{1v} and Δ_{2v}, respectively.

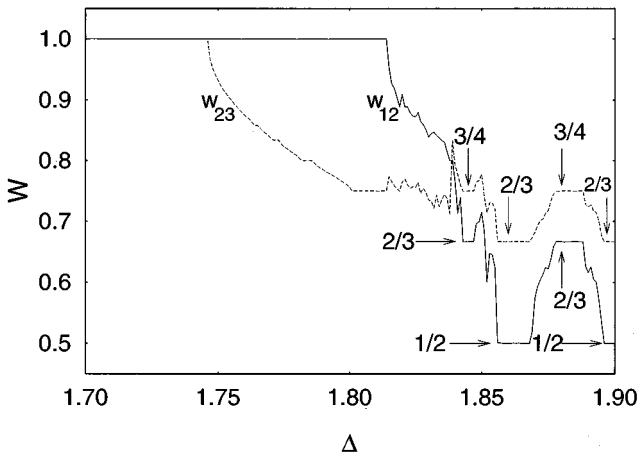

FIG. 4. Variation of the winding number w_{rs} as a function of the gradient Δ, for $i=1.9$, in a 2×3 array. The existence of the (1/2, 2/3) and (2/3, 3/4) frequency-locked regions is clearly seen for two disjoint domains of Δ.

1-0 and 2-0 however continue to remain synchronous all the way out to $\Delta=\Delta_{2v}(i)$ [barring a small Δ interval, in which mode locking occurs when both ω_{12} and ω_{23} are rationals $\in(0,1)$]. The difference in the critical values, Δ_{1v} and Δ_{2v}, decreases as the value of i is increased and eventually the phase locking between both pairs of junctions becomes unstable simultaneously. The values of Δ_{1v} and Δ_{2v}, for different i, define curves in the (i,Δ)-parameter space, which start out from the steady-state boundary as distinct, but eventually merge together for large values of i (see Fig. 2). The system shows voltage locking in the entire $0<\Delta<\Delta_{1v}(i)$ domain, *outside* the steady-state region.

Between the Δ_{1v} and Δ_{2v} curves (see Fig. 2), we see the clear existence of various mode-locked tongues, all of which emanate from the steady-state curve boundary and terminate on the Δ_{2v} curve. In between these tongues, the behavior is quasiperiodic with two independent frequencies (QP^2), much as for an overdamped triangle driven by independent current sources.[18] This similarity of behavior is no coincidence. Indeed, with junctions 1-0 and 2-0 mode locked, the system behaves effectively like the overdamped triangle and the phase diagram of the former has embedded within it the entire phase diagram of the latter. This further implies that the quasiperiodicity with three frequencies (QP^3) and chaos feasible for this system all occur outside this region, as indeed they do.

The frequency locking for $\Delta>\Delta_{2v}(i)$ is characterized by two winding numbers $(w_{12},w_{23})\equiv(p_1/q_1,\ p_2/q_2)$. These correspond to the two pairs of junctions 1-0, 2-0 and 2-0, 3-0, respectively. (In the region between Δ_{1v} and Δ_{2v}, $p_1/q_1=1$ while p_2/q_2 takes on different values, such that $p_1=q_1=p_2$.). At large values of the parameters i and Δ, the nonlinearities of the system become insignificant and the resulting equations can then be solved exactly. From Eqs. (3), the winding numbers w_{12} and w_{23} can be determined, to zeroth order, to have values $(i+3j)/(2i+2j)$ and $(2i+2j)/(3i+j)$, respectively. The motion is largely QP^3 in this asymptotic limit. This statement holds as we move inward from infinity in the parameter space, so long as the nonlinear sine terms are not of the same order as the external applied currents. The mode-locked regions with values of winding number other than $w_{12}=1$ are relatively rare, presumably, because the condition of *pairwise* mode locking is difficult to satisfy. [This immediately becomes clear if we work out the asymptotic values of (w_{12},w_{23}) for various j/i demanding as we do so, that p_1,q_1,p_2,q_2 be small integers]. The mode-locking regions, which are clearly manifest in our numerical simulations, all have (w_{12},w_{23}) values which are ratios of small integers with $q_1=p_2$. In Fig. 4, we display the clear existence of periodic regions corresponding to (2/3, 3/4) and (1/2, 2/3). It is interesting to note that each of these regions exists for two distinct domains of the parameter Δ, i.e., they reappear for higher values of Δ. Hence, each of these tongues is forked.

We have, on occasion, observed period doubling at the edges of these tongues, e.g., for $i=1.9$ and $\Delta=1.846$. The winding number remains unchanged as the bifurcation sequence advances but the period doubling can be deduced from the projection of the phase space trajectories on any 2D subspace of the three torus. The system switches from a trajectory which is 2π periodic to one which is 4π periodic, and so on. After the kth bifurcation, the dc voltages across the bonds r-0, i.e., $\langle\dot{\phi}_r\rangle^{(k)}\rightarrow2^k\langle\dot{\phi}_r\rangle^{(0)}$ $(r=1,2,3)$. We observe, within our numerical resolution, only a few low-order doublings (typically three or four) before the system becomes chaotic. Similar phenomena are observed in the case of an underdamped triangle driven by independent dc current sources.[27]

The dynamics of the system in terms of vortices can be inferred from the behavior of the latter in each of the plaquettes *separately*. The region, $\Delta<\Delta_{1v}(i)$, and outside the fixed-point regime, corresponds to periodic nucleation of vortices at the $y=0$ edge (bond 3-0) followed by their motion in a direction perpendicular to the externally applied current. This results in a well-defined 1/1 limit cycle with a period which exactly matches that of vortex nucleation. In the region between $\Delta_{1v}(i)$ and $\Delta_{2v}(i)$, the drive is able to inject/extract vortices through the bond 2-3 but not through bond 1-2. The dynamics is now governed by the interaction

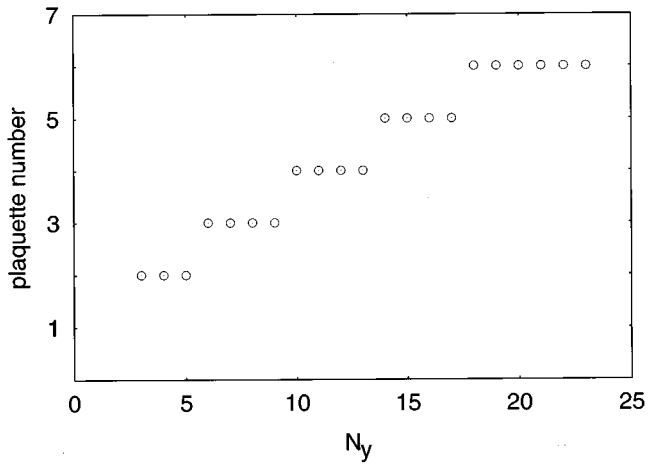

FIG. 5. Plaquette number through which vortices first get injected by the drive as a function of the length of the column. This injection channel is stable at a given plaquette over a range of N_y, as is evident from the steps.

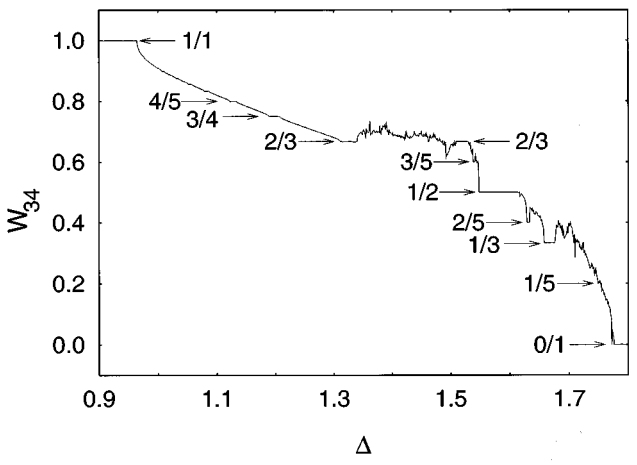

FIG. 6. Variation of the winding number w_{rs} as a function of the gradient Δ, for $i=1.8$ and $N_y=7$. The existence of the mode-locked regions is evident as for $N_y=3$ but over much smaller ranges in Δ.

of these vortex flows — one in the direction of current, the other perpendicular to it — and the observed quasiperiodicity with two independent frequencies is, in fact, an outcome of the interaction of the two associated independent time scales. For mode locking [characterized by $(w_{12},w_{23})=(1,p_2/q_2)$] in this region, the number of vortices injected by the drive through bond 2-3 in each repeating sequence of q_2 vortices is precisely q_2-p_2.[18] Since there is no flow of vortices across bond 1-2, all the vortices, that leave the second plaquette through bond 2-0, have also to pass through bond 1-0. Hence, $p_1=q_1=p_2$, as observed. For $\Delta>\Delta_{2v}(i)$, the drive starts injecting additional vortices through bond 1-2. As a result, we have three independent frequencies (time scales) existing in the system. This is also the minimum number required for a system to display chaos. The interplay among these three frequencies can thus produce any one of P, QP^2, QP^3 or chaos. For drive parameters inside a frequency-locked tongue, the drive injects q_2-p_2 vortices through bond 2-3 and q_1-p_1 vortices through bond 1-2 in such a way that the locking is stable.

The existence of the critical parameters Δ_{1v} and Δ_{2v} shows up additionally in the variation of the time-averaged vortex occupancy $\langle n_- \rangle$ of negative vortices in *any* plaquette as a function of the injected vorticity, Δ. The occupancies $\langle n_-^1 \rangle$ and $\langle n_-^2 \rangle$ show sharp jumps from zero, at Δ_{2v} and Δ_{1v}, respectively. A similar study for positive vortices allows us to associate the corresponding discontinuities with the edges of the mode-locked tongues.

Many of the qualitative features of this configuration carry over to a longer column of Josephson junctions driven by a linear current profile. As the length of the column is increased, the region of voltage locking characterized by a gradient value Δ_{1v}, decreases. It is interesting to pinpoint the pair of junctions where the phase locking first breaks and vortex injection across the drive edge takes place. We show this in Fig. 5. More precisely, we plot the number of the plaquette into which a vortex is first injected by the drive (or equivalently that of the y bond connecting the pair of junctions across which phase locking first breaks) as a function of N_y. The point of injection is located at the second plaquette from the top (the region with low current bias) to start with, but shifts downwards as N_y is increased. The figure shows well-defined steps in the plaquette number, i.e., the injection always takes place through a given plaquette for a range of values in N_y. The breakdown gradually shifts to a plaquette away from the edges only when N_y exceeds a critical value. After one of the junctions has become mode *un*locked, the next to follow suit are the adjacent ones, on the drive edge. The breakdown continues alternately until phase locking for all junctions in the column is broken. This sequence of breakdowns is characterized by $\{\Delta_{rc}\}$, $r=1,2,\ldots,N_y-1$.

For $N_y>3$, the system shows locking with winding numbers even less than 1/2, in the region between Δ_{1v} and Δ_{2v}. For example, consider the case, $N_y=7$, for which the voltage locking in the column breaks first at the bond 3-4 (see Fig. 5). In Fig. 6, we have accordingly shown the variation of w_{34} with Δ. We clearly see that the winding number w_{34} has plateaus at various rationals between *zero* and unity. The winding number 0 corresponds to the case where junction 3-0 is executing harmonic motion while junction 4-0 is running.

B. $N_x\times 2$ ladders

We now investigate the behavior of JJA's, which have $N_y=2$ but are extended along the x direction, i.e., in the direction of the injected current. To start with, we take $N_x=3$ and once again we set $\phi_0=0$ (see inset of Fig. 7).

The schematic phase diagram for this configuration is shown in Fig. 7. This contains prominent regions of steady-state (SS) and QP^2 behavior. In addition, we see the existence of two well-defined boundaries at $\Delta_{1h}(i)$ and $\Delta_{2h}(i)$, whose significance is best understood from the $\langle w_{rs} \rangle$ *versus* Δ plot, given in Fig. 8, for $i=1.8$. In interpreting this diagram, it is useful to recall that for $\Delta=0$, two rows of junctions decouple, by symmetry, and the whole array behaves like a single Josephson junction. From Eqs. (3), this clearly corresponds to $\phi_1=\phi_3$, $\phi_2=\phi_4$, and $\phi_1=2\phi_2$, i.e., to $w_{13}=w_{24}=1$ and $w_{12}=w_{34}=1/2$. In other words, the junctions in each column are perfectly synchronous (winding

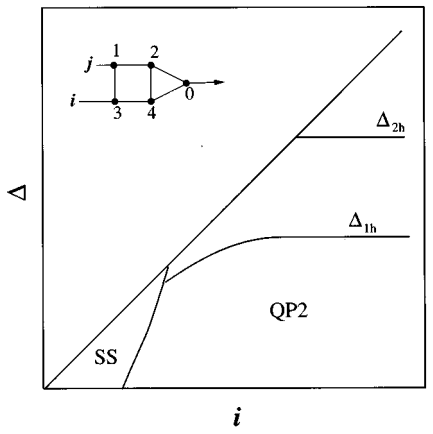

FIG. 7. Schematic phase diagram (not to scale) for a 3×2 configuration shown in the inset ($\phi_0=0$, by choice). The region marked SS is the steady-state region. The region for $\Delta<\Delta_{1h}(i)$ corresponds to quasiperiodic behavior with two frequencies. The boundaries $\Delta_{1h}(i)$ and $\Delta_{2h}(i)$ represent the loss of phase locking in the first and second columns, respectively.

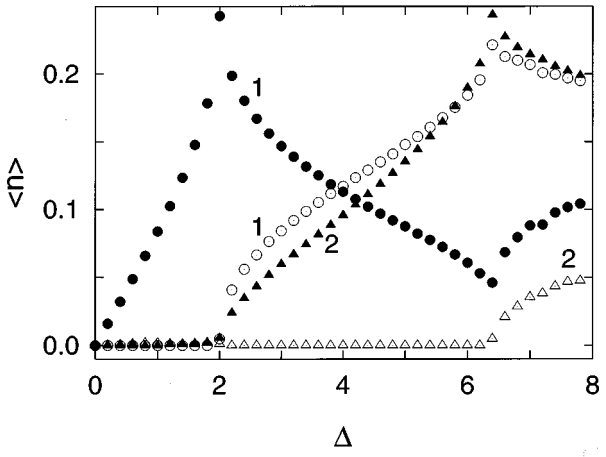

FIG. 9. Variation of the time-averaged vortex occupancy $\langle n_{\pm}\rangle$ with Δ for $i=8.0$. The filled symbols corresponds to positive vortices, while the open ones represent negative vortices. The numbers marked against various sets of data denote the plaquette concerned. The discontinuities occur at $\Delta_{1h}=2.0$ and $\Delta_{2h}=6.4$.

number unity), while those across neighboring columns are mode locked with rational winding numbers. For finite Δ, the phase locking along the columns, characteristic of the $\Delta=0$ line, continues and is stable. However, the mode locking between junctions in neighboring columns breaks and their relative motion is now characterized by an irrational winding number. Hence, the ''completely inphase'' solution (*all* winding numbers rational) observed earlier in Sec. III A, does not exist in the strict sense here, for $\Delta>0$.

Instead, the motion is largely quasiperiodic with two independent frequencies f_1 and f_2. Each of these frequencies increases in magnitude with i but their difference f_1-f_2 decreases. From Fig. 8, we note that the locking between the voltages at sites 1 and 3 breaks at $\Delta_{1h}=2$ and the winding number w_{13} thereafter starts decreasing continuously. The voltages at sites 2 and 4, however, remain locked until a much higher value $\Delta_{2h}(=6.4)$ of Δ. As Δ is increased further, both winding number ratios, w_{13} and w_{24}, decrease.

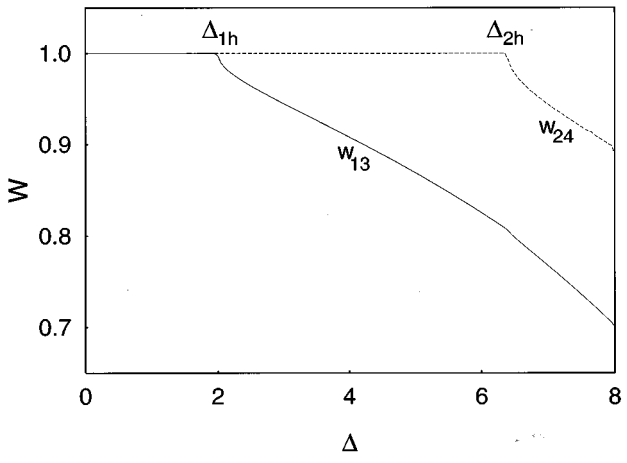

FIG. 8. Variation of the winding number w_{rs} as a function of the gradient Δ, for $i=8$ in a 3×2 array. $\Delta_{1h}(i)$ and $\Delta_{2h}(i)$ are the critical values at which the phase lockings in the columns break.

The behavior of the system now also shows QP[3]/chaos. The frequency-locked zones, which exist in large measure for the $2\times N_y$ ladders, are very rare for the 3×2 case. It is noteworthy that in the parameter region, $0<\Delta<\Delta_{2h}(i)$, this configuration can be thought of as the overdamped triangle with the (apparent) reference point (bond 2-4) itself undergoing periodic motion. The latter tends to wash out all rational lockings between voltages at sites 1 and 3, other than $w_{13}=1$.

To gain further insights, we focus on the behavior of vortices in this system. The time average of the vortex occupancy (both positive and negative), $\langle n_{\pm}\rangle$, in a given plaquette, as a function of the injected vorticity, Δ, is shown for plaquette 1 in Fig. 9. For $\Delta<\Delta_{1h}$, the density of negative vortices in this plaquette is negligible, i.e., there is no injection/extraction of vortices by the drive. However, positive vortices nucleate at the $y=0$ edge for $\Delta>0$. They enter through the bond 3-4 and leave through the bond 1-2. The vortex occupancy of positive vortices keeps increasing until $\Delta=\Delta_{1h}$. For $\Delta>\Delta_{1h}$, the drive starts injecting negative vortices and sucking out positive ones. This is evident from the sharp increase in $\langle n_-\rangle$, and the accompanying decrease in $\langle n_+\rangle$, in the first plaquette. This trend continues until the value $\Delta=\Delta_{2h}$ is reached. As Δ is increased beyond Δ_{2h}, $\langle n_-\rangle$ gradually decreases and tends to saturate, while $\langle n_+\rangle$ starts increasing again.

In plaquette 2, which is further away from the drive edge, the variation of $\langle n_{\pm}\rangle$ with Δ follows a different pattern (see Fig. 9). Viewed at higher resolution, this figure shows that, for $\Delta<\Delta_{1h}$, the negative vortex occupancy of this plaquette, $\langle n_-^2\rangle$, is very low while $\langle n_+^2\rangle$ is strictly zero. The negative vortices enter through bond 2-0 and exit through bond 4-0. Once Δ exceeds Δ_{1h}, this flow of negative vortices stops and $\langle n_-^2\rangle$ drops to zero. On the other hand, positive vortices now start nucleating at the $y=0$ edge. They enter the array through bond 4-0 and annihilate with their images at bond 2-0. Their number increases with increase in Δ and peaks at Δ_{2h}. For $\Delta>\Delta_{2h}$, $\langle n_-^2\rangle$ registers a sharp increase, while $\langle n_+^2\rangle$ begins to decay gradually.

It may be noted that the magnitude of the maximum negative vortex occupancy in plaquette 1 is about a factor of 5 higher than that in the plaquette 2. Furthermore, the two critical values of Δ, viz. Δ_{1h} and Δ_{2h}, identified by the loss of phase locking in the first and second columns, respectively, are sharply demarcated by transitions in the vortex (both positive and negative) occupancies in the two plaquettes. They represent the threshold values of Δ required to inject vortices along the direction of the current, into plaquettes 1 and 2, respectively. One could, alternatively, think of plaquette 2 in this configuration as being driven by plaquette 1 *via* an ''effective'' time-dependent current source. This way of viewing the system makes the similarity in the behavior of $\langle n_{\pm}\rangle$ in plaquette 2 for $\Delta\in[\Delta_{1h},\Delta_{2h}]$ to that in plaquette 1 for $\Delta\in[0,\Delta_{1h}]$ plausible.

It is of interest at this stage to point out that the vortex flows we have mapped provide natural explanations for several observations made by Mehrotra and Shenoy[3] on the 4×3 array they studied. These authors plotted the bond power spectra $S_{rs}(\omega)=|\dot{\phi}_{rs}(\omega)|^2$, i.e., the Fourier transform of the voltage time series $\{\dot{\phi}_{rs}(t)\}$, as also the vortex spectrum, $C(\omega)$, obtained by Fourier transforming the vortex-vortex correlation function $C_{\pm\pm}(t)=\langle N_{\pm}^{T}(t)N_{\pm}^{T}(0)\rangle$, where $N^{T}(t)$ is the total number of vortices in the array. They verified that in the QP^3 regime, both spectra have prominent peaks at exactly matching frequencies $f_r(r=1,2,3)$ and that all higher frequency peaks are the harmonics of f_r. Examining next the distribution of vortex-appearance times in various plaquettes, i.e., the time intervals between consecutive changes from zero to nonzero vortex occupancy, they found this to be sharply peaked at values, $\tau_r(r=1,2,3)$, *which were precisely the inverse frequencies of the peaks in the voltage spectra, i.e.,* $\tau_r=f_r^{-1}$.

These observations can all be straightforwardly understood in terms of the periodic flow of vortices along the individual columns, discussed by us in this paper. Indeed, the periodicity of the flow ensures that a vortex appears at well-defined intervals in a given plaquette. Since these flows are always accompanied by changes in the ϕ_r, they invariably induce voltages which are transmitted to all points of the array because the coupling between junctions is long range. The (inverse) periods associated with these flows are hence seen in all spectra related to the system. To see why no other frequencies are seen, we note that a system of overdamped junctions cannot sustain either inertial oscillations or single junction chaos. In addition, if the array is dc driven, no external frequencies are introduced. Thus, any frequency or chaos generated in the system *must* result from the collective behavior and nonlinear dynamics of the array as a whole. The frequencies both discrete (QP^2) and continuous (chaos) must, therefore come exclusively from vortex flows, or more specifically, vortex lifetimes.

It may be further noted that the mixing of vortices flowing along columns, with those injected by the drive invariably produces vortex-antivortex annihilation *inside* the array, in addition to those at its boundaries. This generates vortex lifetimes over a continuous range. Consequently, there is a substantial rise in the noise background in both the voltage and vortex spectra and a broadening in the distribution of vortex-appearance times. This had been noticed in Ref. 3 and diagnosed as a signature of chaos.

The behavior of the $(N_x\times2)$ ladder for $N_x>3$ has many of the features discussed above for $N_x=3$. For all N_x, the locking in columns breaks sequentially, starting at the drive edge and moving towards the busbar, as the value of Δ is increased. These breakdowns are characterized by $\{\Delta_{rh}\}$, $r=1,2,\ldots,N_x-1$. The values of Δ_{rh}, for different values of i, form distinct boundaries in the (i,Δ) phase diagram. The behavior of the system changes qualitatively across each of these boundaries, which are, interestingly enough, invariant with respect to an increase in N_x, i.e., incrementing N_x by unity adds one new critical parameter Δ_{N_xh} to the sequence, but leaves the rest of it unaltered. Moreover, for a given N_x, $\Delta_{rh}-\Delta_{(r-1)h}>\Delta_{(r-1)h}-\Delta_{(r-2)h}$. For example, the critical Δ values corresponding to breakdown in the first four columns are given by 2.0, 6.4, 23.2, 96.1, respectively.

The breakdowns continue to be equally well marked by discontinuous jumps in the positive as well as negative vortex occupancy of various plaquettes, as functions of Δ. For values of Δ below Δ_{rh}, the motion of vortices in the direction of the external current is confined to the first $(r-1)$ plaquettes, counting from the drive edge. Their motion in the remaining columns is perpendicular to this current. Increasing Δ beyond Δ_{rh} injects vortices into the rth plaquette and leads to a ''mixing'' of positive and negative vortices there. The larger the value of r, the (disproportionately) higher the associated threshold, Δ_{rh}, for vortex injection. Finally, it may be mentioned that, with these vortex flows in place, each plaquette in the ladder can be thought of as being driven by an effective time-dependent current source to its left, and having a periodically oscillating reference point to its right.

C. Higher-order quasiperiodicity and chaos

In the previous section, we saw explicitly that in the time-dependent $\Delta<\Delta_{1h}$ regime, the 3×2 ladder has two independent frequencies f_1 and f_2, *localized* spatially in plaquettes 1 and 2, respectively. An extension of this behavior in ladders with $N_x>3$ opens up the possibility of sustaining QP^N $(N>3)$ in such systems. In Fig. 10, we show the voltage power spectrum for $N_x=5$ at $(i,\Delta)=(1.9,\ 1.78)$. The spectrum contains four independent frequencies $f_1=0.075\ 07$, $f_2=0.025\ 15$, $f_3=0.022\ 49$, and $f_4=0.022\ 31$ with an uncertainty of $\pm0.000\ 03$. All other spectral frequencies can be expressed as linear combinations of these four. Although it is conceivable that, for suitable values of i and Δ, two or more of these frequencies may lock, to produce quasiperiodicity of lower order, our investigations indicate that $f_3\to f_4$ only as $i\to\infty$. The issue can, unfortunately, not be settled numerically because its resolution requires spectra of voltage time series, whose length eventually becomes prohibitive.

A plot of the distribution of vortex-appearance-time intervals confirms that these frequencies are associated with the four plaquettes in the ladder and correspond to vortex motion perpendicular to $i_{\rm ext}$. For $\Delta>\Delta_{1h}$, the drive is able to inject vortices into the first plaquette, and to thereby introduce new time scales in the system. The onset of chaos for $\Delta>\Delta_{1h}$ occurs as a result of interaction between vortex flows in the direction of, and perpendicular to, the current. A similar phe-

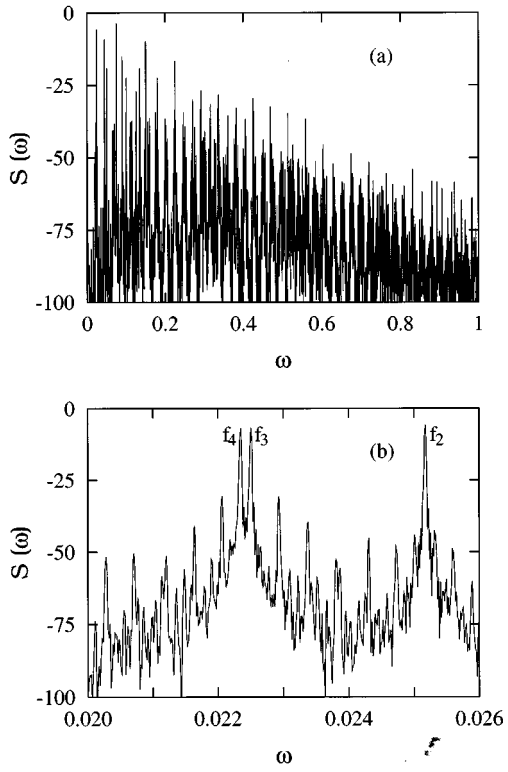

FIG. 10. (a) The voltage power spectrum and (b) a magnified portion of it, for a 5×2 array with $i=1.9$ and $\Delta=1.78<\Delta_{1h}$. The spectrum has four frequencies at $f_1=0.075\,07$ (not shown), $f_2=0.025\,15$, $f_3=0.022\,49$, and $f_4=0.022\,31$ and linear combination of these four frequencies. The frequencies f_3 and f_4 are resolved from runs of typically 10^6 steps.

nomenon is observed for $N_x=6$, where we see five independent frequencies with f_4-f_5 much smaller than f_3-f_4.

To conclude, an $N_x\times2$ ladder *can*, for $\Delta<\Delta_{1h}$, sustain higher order quasiperiodicity with (N_x-1) *noninteracting* frequencies. This behavior becomes unstable as soon as, for $\Delta>\Delta_{lh}$, a new *interacting* frequency is introduced. In $(2\times N_y)$ ladders interactions are unavoidable from the very outset, and the system inevitably passes from QP^3 to chaos.

D. $N_x\times N_y$ arrays of Josephson junctions

Having studied the $2\times N_y$ and $N_x\times2$ lattices, we look at *general* $N_x\times N_y$ arrays, whose behavior has features of both ladders. For $\Delta=0$, the array equations have the solution: $\phi_r=\phi_{r+N_x-1}$ and $\phi_1=2\phi_2=\ldots=(N_x-1)\phi_{N_x-1}$. As Δ is increased, the locking between junctions in each column is initially retained, while that between junctions in different columns is broken. [The existence of columnwise locking has also been reported for uniformly driven arrays with disorder in i_c (Ref. 9)]. This corresponds to vortices nucleating at the $y=0$ edge of each column, moving up the latter to the $y=L_y$ edge and annihilating there. The (N_x-1) noninteracting vortex flows, which thus come into existence, lead to quasiperiodicity with (N_x-1) independent frequencies.

The subsequent pattern of mode *un*locking, under a continuous increase in Δ, is quite interesting: The first bond to unlock is the one at the center of the drive edge (henceforth numbered 1). This is followed by those adjacent, and then by

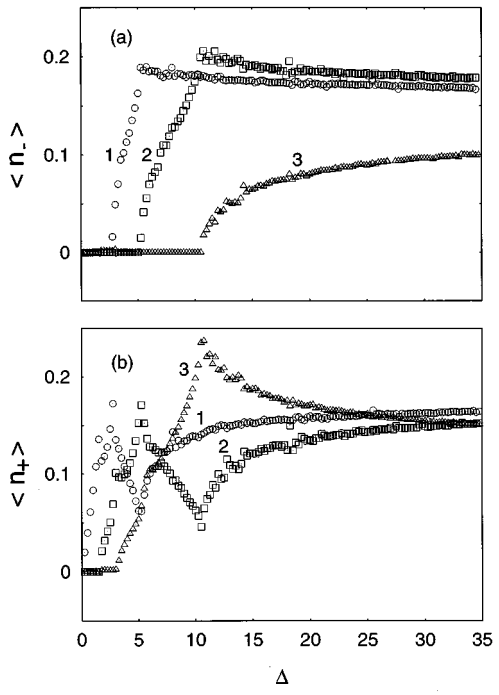

FIG. 11. Variation of the time-averaged vortex occupancy $\langle n\rangle$ with Δ, for $N_x=N_y=4$ and $i=35.0$. The numbers marked against various sets of data denote the plaquette concerned. The behavior of $\langle n\rangle$ for all plaquettes in a column, for either sign of vortices, is similar.

the central bond of column 2. More bonds now give way, symmetrically, in column 1, and likewise in column 2, before the central bond of column 3 loses synchronicity. The set of bonds which come unlocked thus has, for all sufficiently large values of Δ, the shape of an isoceles triangle with one or three junctions at the leading edge. (This was verified by running on a large, 32×32, lattice). Since a new channel of vortex injection opens up each time a bond is unlocked, this is also the region of maximal mixing and turbulence. Finally, our numerical studies indicate that the value of Δ, at which the locking breaks in a given column, decreases, quite generally, with N_y.

As before, the breakdowns are well marked by sharp variations in the time-averaged vortex occupancies, $\langle n_\pm\rangle$, as functions of Δ. These are shown in Fig. 11, for the topmost row of a 4×4 array (see Fig. 1). (The qualitative behavior of $\langle n_\pm\rangle$ for the other rows is similar). As for the 4×2 ladder, there are three critical values of Δ (2.75, 5.25, and 11.0, in this case) associated with loss of voltage locking between sites in columns 1, 2, and 3, respectively. The value of Δ at which vortices begin to flow in, through the central bond of the drive edge, is 1.5, for comparison.

IV. SUMMARY AND DISCUSSION

To summarize, we have studied the onset of chaos in 2D JJA's at zero temperature and zero magnetic field. By choosing all array junctions to be overdamped, we have excluded individual junction oscillations and focused on collective effects arising exclusively from interactions between junctions. We find that in the time-dependent regime, the system un-

dergoes a series of dynamical transitions, as we increase the injected vorticity. The transitions are all amenable to a dual interpretation. From the viewpoint of the basic field variables, ϕ_r, these are mode-locking, or rather mode-*un*locking, transitions. From the standpoint of collective excitations, these transitions are marked by the flow of vortices through the junctions which have come unlocked.

At values of the external current, for which the junctions along the drive edge are 1/1 mode locked, vortices flow exclusively along columns, and the system exhibits (N_x-1) independent frequencies. Some of these frequencies can, in principle, be commensurate. In practice, however, this seems to happen very rarely. So much so that we have, in fact, never encountered an attractor lower than QP^N. It is, nevertheless, of interest to look for regions of parameter space, where the system displays $\mathrm{QP}^{N_x-1}, \ldots, \mathrm{QP}^1$ equivalent to P behaviors, particularly with a view to determining whether they are connected via a continuous path. For if they are, we would arrive at a route to chaos which passes through each of $\mathrm{QP}^1, \ldots, \mathrm{QP}^N$, in partial vindication of the Landau conjecture.[22]

To trace vortex paths in their entirety, it is expedient to view an array with free boundaries in an alternative way, namely, as one half of an array of double length in the direction perpendicular to the external current drive. In the double length array, the dynamics is constrained to be antisymmetric around the middle and the image system now has periodic boundary conditions. In this extended lattice, the vortex number is strictly conserved, i.e., vortices always nucleate and annihilate in pairs and all the frequencies generated in the system correspond to vortex lifetimes. Moreover, vortex motion is effected by changes in ϕ values, which induce nonzero Ohmic voltages in the array. Owing to the long-range interaction, or equivalently, the global coupling between junctions, any vortex motion is sensed by every array site. The same peaks are consequently seen in the Fourier transforms of the voltage time series, no matter where the voltage is measured. The height of a given peak, however, depends on the distance between the bond chosen for the voltage measurement, and the path followed by the vortex responsible for that peak.

It is also intuitively clear why mixing is so efficient at producing new frequencies: In its absence, vortices, after nucleating at the free boundaries, have to traverse the entire length of the column before being annihilated by *image* antivortices. By contrast, once the option of mixing opens up, annihilations can additionally occur on much shorter time scales in the bulk of the array. As a result, lifetimes can be generated over an essentially continuous range of values. The quantitative study of mixing as also the connection between the resultant vortex flows and the chaotic attractor are clearly topics for future research and have not been dealt with in this paper.

Finally, we have supplemented the above picture with maps of the parameter space associated with these systems. For arrays consisting of single columns, we clearly discern mode-locked Arnold tongues, which overlap in the chaotic regime. Furthermore, the phase diagram for the 2×3 case, for example, has, nested inside it, that of the 2×2 triangular network. Not surprisingly, for parameter values corresponding to the nesting, one of the bonds is closed (through 1/1 mode locking) to vortices. All the tongues outside this region seem to be forked.

To conclude, our work has provided explanations for a number of correlations, pointed out by Mehrotra and Shenoy,[2,3] between phase and vortex diagnostics. It has, moreover, generalized the results of Das *et al.*[18] pertaining to a triangular network of Josephson junctions. It has placed vortex flows, discussed by Xia and Leath[4,5] in the context of the breakdown of superconductive flow in JJA's, in a much wider framework and given them a much greater significance. Lastly, it has expanded, in some nontrivial ways, on the theme of mode locking, earlier dealt with for harmonically driven Josephson junctions or pendula by Bak and co-workers,[34,35] among others. It has, therefore, we believe, synthesized a number of seemingly independent investigations into a single coherent picture of array dynamics.

[1] J. P. Eckmann, Rev. Mod. Phys. **53**, 643 (1981).
[2] R. Mehrotra and S. R. Shenoy, Europhys. Lett. **9**, 11 (1989).
[3] Ravi Mehrotra and Subodh R. Shenoy, Phys. Rev. B **46**, 1088 (1992).
[4] W. Xia and P. L. Leath, Phys. Rev. Lett. **63**, 1428 (1991).
[5] P. L. Leath and W. Xia, Phys. Rev. B **44**, 9619 (1991).
[6] K. K. Mon and S. Teitel, Phys. Rev. Lett. **62**, 673 (1989).
[7] F. Falo, A. R. Bishop, and P. S. Lomdahl, Phys. Rev. B **41**, 10 983 (1990).
[8] Sujay Datta, Shantilal Das, Deshdeep Sahdev, and Ravi Mehrotra, Mod. Phys. Lett. **10**, 451 (1996).
[9] C. B. Whan, A. B. Cawthorne, and C. J. Lobb, Phys. Rev. B **53**, 12 340 (1996).
[10] P. Hadley, M. R. Beasley, and K. Wiesenfeld, Phys. Rev. B **38**, 8712 (1988).
[11] A. S. Deakin and M. A. H. Nerenberg, Phys. Rev. B **25**, 1559 (1982).
[12] D. W. Jillie, M. A. H. Nerenberg, and J. A. Blackburn, Phys. Rev. B **21**, 125 (1980).
[13] M. A. H. Nerenberg, J. A. Blackburn, and D. W. Jillie, Phys. Rev. B **21**, 118 (1980).
[14] Y. D. Dai and Y. H. Kao, J. Appl. Phys. **52**, 4135 (1981).
[15] L. G. Neumann, Y. D. Dai, and Y. H. Kao, Appl. Phys. Lett. **39**, 648 (1981).
[16] R. K. Tavakol and A. S. Tworkowski, Phys. Lett. **100A**, 65 (1984); **100A**, 273, (1984); Phys. Lett. **111A**, 317 (1985).
[17] A. K. Jain, K. K. Likharev, J. E. Lukens, and J. E. Sauvageau, Phys. Rep. **109**, 310, (1984).
[18] Shantilal Das, Sujay Datta, Mitrajit Dutta, Shilpa Jain, and Deshdeep Sahdev, Physica D **91**, 278 (1996); Shantilal Das, Sujay Datta, M. K. Verma, Deshdeep Sahdev, and Ravi Mehrotra, *ibid*. **91**, 292 (1996).
[19] F. Ichikawa, T. Aomine, and S. Hosogi, J. Appl. Phys. **63**, 5 (1988).
[20] F. Ichikawa and T. Aomine, J. Appl. Phys. **66**, 1 (1989).
[21] E. Hopf, Commun. Pure Appl. Math. **1**, 303 (1948).
[22] L. Landau and E. Lifshitz, *Fluid Mechanics* (Pergamon, Oxford, 1959).

[23] D. Ruelle and F. Takens, Commun. Math. Phys. **20**, 167 (1971).
[24] S. Newhouse, D. Ruelle, and F. Takens, Commun. Math. Phys. **64**, 35 (1978).
[25] C. Grebogi, E. Ott, and J. A. Yorke, Phys. Rev. Lett. **51**, 339 (1983); Physica D **15**, 354 (1985).
[26] By C^K it is meant that given any ϵ, a perturbation can be found such that it and all its derivative up to order K are less than ϵ.
[27] Shantilal Das, Sujay Datta, and Deshdeep Sahdev, Physica D **101**, 333 (1997).
[28] W. C. Stewart, Appl. Phys. Lett. **12**, 277 (1968).
[29] D. E. McCumber, J. Appl. Phys. **39**, 3113 (1968).
[30] S. R. Shenoy, J. Phys. C **18**, 5163 (1985); **20**, 2479(E) (1987).
[31] H. Eikmans and J. E. van Himbergen, Phys. Rev. B **41**, 8927 (1990); H. Eikmans, J. E. van Himbergen, H. S. J. van der Zant, K. de Boer, and J. E. Mooij, Physica B **165 & 166**, 1569 (1990).
[32] D. Dominguez, J. V. José, A. Karma, and C. Wiecko, Phys. Rev. Lett. **67**, 2367 (1991).
[33] Sujay Datta, Shantilal Das, Deshdeep Sahdev, Ravi Mehrotra, and Subodh Shenoy, Phys. Rev. B **54**, 3545 (1996).
[34] M. H. Jensen, P. Bak, and T. Bohr, Phys. Rev. A **30**, 1960 (1984).
[35] T. Bohr, P. Bak, and M. H. Jensen, Phys. Rev. A **30**, 1970 (1984).